

Chronic pain detection from resting-state raw EEG signals using improved feature selection

Jean Li, Dirk De Ridder, Divya Adhia, Matthew Hall, Jeremiah D. Deng *Member, IEEE*

Abstract—We present an automatic approach that works on resting-state raw EEG data for chronic pain detection. A new feature selection algorithm - modified Sequential Floating Forward Selection (mSFFS) - is proposed. The improved feature selection scheme is rather compact but displays better class separability as indicated by the Bhattacharyya distance measures and better visualization results. It also outperforms selections generated by other benchmark methods, boosting the test accuracy to 97.5% and yielding a test accuracy of 81.4% on an external dataset that contains different types of chronic pain.

Index Terms—Feature selection, resting-state EEG, chronic pain.

I. INTRODUCTION

Pain is defined as an unpleasant sensory and emotional experience associated with actual or potential tissue damage or described in terms of such damage [1]. While acute pain can be recognized as a symptom of an underlying problem, chronic pain, which extends beyond the period of healing from the original insult or injury, lacks the acute warning function of physiological nociception [2]. The International Association for the Study of Pain and International Classification of Diseases (ICD11) has defined chronic pain as pain that extends beyond three months, irrespective of the cause. Therefore, chronic pain can be considered not a mere symptom of another disease, but a health condition by itself [3], [2]. Indeed, chronic pain is not simply a temporal extension of acute pain but involves distinct mechanisms [4]. Chronic pain is associated with multiple other symptoms. Despite being associated with physical conditions such as cardiovascular disease [5], chronic pain also correlates with cognitive dysfunction such as difficulties in attention, learning, memory, and decision making [6]. About 1/3 of the patients who suffer from chronic pain display other symptoms such as a combination of irritability, depression, anxiety, and sleep problems [7], [5], [8].

Chronic pain and its co-morbidities lead to increased disability [9], carrying the highest global burden associated with disability [10]. The correlation between chronic pain and disability creates a huge cost to society (\$560-635 billion per year), far more than heart disease, cancer, and diabetes [11], and back pain alone amounts to 1.7% of the global national product every year [12]. Chronic pain is a worldwide problem.

J. Li and J. D. Deng are with the Department of Information Science, University of Otago, Dunedin 9054, New Zealand.

D. De Ridder, D. Adhia and M. Hall are with the Department of Surgical Sciences, School of Medicine, University of Otago, Dunedin 9054, New Zealand.

Corresponding author: J. D. Deng, email: jeremiah.deng@otago.ac.nz

Studies have found that the prevalence of chronic pain is 20%, both in the USA [13] and Europe [7], and around 30% in China [8], which is similar to the prevalence in low-income and middle-income countries [14]. High-impact chronic pain, which occurs in 8% of the population, frequently limits patients' life or work activities [13]. Due to the lack of effective, specific, and safe therapies, chronic pain remains one of the major causes of human suffering [10]. Many of the currently available pain therapies either are inadequate or cause unpleasantness to patients [15], some even causing deleterious side effects [16], [17].

In research and clinical practice, the gold standard of diagnosing pain is based on self-report. Self-report pain diagnosis could be challenging in certain clinical contexts or conditions. In particular, reliance on self-report of pain can be challenging where there is no evidence of tissue damage, or the presence of tissue damage may not be necessary to determine the presence of pain. Moreover, an objective measure of pain could pave the way to improve diagnostic and treatment outcomes. Therefore, it is necessary to develop simple, reliable, and clinically applicable method that can validate the pain experience and justify the allocation of relevant healthcare services and benefits.

The goal of this study is to find an automatic method to predict chronic pain through resting-state EEG. We focus on functional connectivity rather than activity, as recent studies have suggested the effectiveness of functional connectivity in EEG pain analysis [18], [19], [20], and this may be superior to detecting a pain-generating network [21].

To achieve this goal, we carry out some automatic pre-processing and extract spectral connectivity features. Machine learning then is applied, utilizing feature importance ranking and a novel feature selection technique to build high-performing classification models. Finally, we report the competitive performance gained from a 20-dimension connectivity feature set based on robust cross-validation, visualization, and separability assessments.

II. RELATED WORK

Multiple previous studies have shown the effectiveness of pain prediction through EEG using machine learning methods. Vanneste *et al.* [22] has yielded an accuracy of 92.53% on chronic pain through a support vector machine (SVM) trained on regions of interest. Nezam *et al.* [23] applied a SVM on selected band power features and reported an accuracy of $83\pm 5\%$ and $62\pm 6\%$ for the three and five pain levels respectively. Vuckovic *et al.* [24] predicted central neuropathic pain based on the resting-state EEG and reported an accuracy

of 85% with a simple linear classifier using band power features. Vijayakumar *et al.* [25] investigated quantifying tonic thermal pain across healthy subjects. By using time-frequency wavelet representations of independent components obtained from EEG, their random forest model achieved an accuracy of 89.45%.

These previous approaches, however, relied on labor-intensive pre-processing for artefact removal, which is expensive and, therefore, cannot be used in routine clinical practice. Therefore, a user-friendly, clinically applicable system is needed that can automatically pick up the neural pain signature on raw, unprocessed data, using a low-cost device.

III. DATA DESCRIPTION

The main data used for this study consist of the EEG recordings of 37 healthy participants, and 37 patients with chronic knee pain. Data were acquired in Dunedin hospital with 19 electrodes in the standard 10–20 international placement (Fp1, Fp2, F7, F3, Fz, F4, F8, T3, C3, Cz, C4, T4, T5, P3, Pz, P4, T6, O1, O2).

In addition, we construct an external dataset from two different sources to test the reliability of the features selected from the main dataset. The first group of pain recordings came from 31 subjects suffering from neuropathic pain, details about data acquisition given in [22]. The second group of pain recordings was from 14 subjects with chronic pain (exact types unknown), taken from the TDBrain dataset [26]. Furthermore, EEG data from 47 healthy subjects were also taken from the TDBrain. Overall, the numbers of healthy and chronic pain subjects included in the external dataset are balanced (47 versus 45).

IV. METHODS

A. Pre-processing and feature extraction

All EEG recordings went through an automatic pre-processing procedure to remove potential artifacts and control volume conduction.

The first 10 seconds of all the recordings were discarded to avoid the “initial drift” noise. A notch filter at 50 Hz to attenuate the power line interference was applied to all data, followed by a high-pass filter of 1 Hz and a low-pass filter of 40 Hz. Each recording was cut into 10-second long epochs and went through an auto-cleaning process to repair epochs by interpolation or excluding them. This is achieved by estimating an optimal global peak-to-peak threshold first, then finding trial-wise bad sensors by estimating a separate rejection threshold for each sensor [27]. Lastly, the current source density transformation that is based on spherical spline surface Laplacian [28] [29] [30] [31] was applied to control volume conduction.

In this study, the EEG connectivity is represented by the corrected imaginary phase locking value (ciPLV) [32], as this metric is robust in the presence of volume conduction, and proved capable of ignoring zero-lag connectivity while correctly estimating nonzero-lag connectivity [32]. In particular, for each pair of channels, the ciPLV across all epochs on chosen frequency ω was computed based on the averages of

the real and imaginary parts of the cross-channel spectrum densities:

$$C(\omega) = \frac{\left| E \left[\frac{\text{Im}(S_{xy}(\omega))}{|S_{xy}(\omega)|} \right] \right|}{\sqrt{1 - \left| E \left[\frac{\text{Re}(S_{xy}(\omega))}{|S_{xy}(\omega)|} \right] \right|^2}}, \quad (1)$$

where $S_{xy}(\cdot)$ is the cross-spectral density for channels x and y , and $E[\cdot]$ denotes averaging over all epochs within a sample.

For every pair of channels, the connectivity across all epochs was computed on the mean frequency value of 5 major brain wavebands. These frequency bands are delta (1 ~ 4 Hz), theta (4 ~ 8 Hz), alpha (8 ~ 12 Hz), beta (12 ~ 30 Hz), and gamma (30 ~ 40 Hz). Each sample is therefore represented by a feature vector of 855 dimensions (171 channel pairs \times 5 bands). The MNE package [33] was applied to compute the spectral connectivity measures.

B. Feature selection

There are two main challenges to selecting features for our study. First, we have a relatively small sample size of 74 and a large number of features at 855. This requires a feature selection approach that can effectively handle high-dimensional problems with limited data. Second, the signals collected from each channel represent a summation of neural activity from a broad region of the brain, resulting in high collinearity between features in sensory space EEG analysis.

Various existing feature selection schemes were examined, including those based on filtering, greedy strategy, and swarm intelligence. Unfortunately, none of these approaches yielded satisfactory results. As a result, we developed a customized feature selection scheme by modifying the sequential floating forward selection (SFFS) method [34]. Like SFFS, we also use a classifier as a *wrapper*. Although our feature method is independent of wrapper choices, we used a support vector machine (SVM) with radial basis function kernels as the classifier/wrapper. For the remainder of this article, we will refer to this modified SFFS scheme as “mSFFS”.

Compared with the classical SFFS algorithm, mSFFS records the winning sets of all numbers of features and always starts forward selection from a historical best set, hence allowing for multiple searching branches. The winning sets are updated along the way of both the forward and backward selection process. Bookkeeping of all searched sets is carried out to speed up the searching process and avoid deadlocks. The feature selection algorithm is presented in Algorithm 1.

To narrow down the search space, a preselection procedure was employed. We calculated the SHAP values [35] using XGBoost [36], and only kept the features with a mean absolute SHAP value greater than a given threshold. We took a lenient setting here and had the threshold set to 0. Depending on the exact situation, a positive threshold value could be considered if a harsher preselection policy is intended.

The number of selected features to be used in modeling will contribute to the complexity of the model, which may affect its generalization ability. We used cross-validation in deciding the optimal number of features because cross-validation is an established, reliable approach in model selection [37]. In our

Algorithm 1: Modified SFFS

Data: K : intended number of features; full feature set \mathcal{F}

Result: Selected feature subset W_K

Preselection:

Calculate SHAP score for all features;
Remove features with SHAP score smaller than 0
from \mathcal{F}

Initialization:

$k \leftarrow 1$;
for $i \in 0:K$ **do**
 winning set $W_i \leftarrow \emptyset$;
 winning set score $s_i \leftarrow 0$
end

Feature set bookkeeping: $\mathcal{B} \leftarrow \emptyset$

while $k \leq K$ **do****Forward selection:**

Find the best feature to add:
 $f \leftarrow \arg \max_f \text{score}(W_{k-1} \cup f)$;
 $\forall f \in \mathcal{F}, (W_{k-1} \cup f) \notin \mathcal{B}$;
Update bookkeeping: $\mathcal{B} \leftarrow \mathcal{B} \cup \{W_{k-1} \cup f\}$;
if $\text{score}(W_{k-1} \cup f) > s_k$ **then**
 Update winning selection: $W_k \leftarrow W_{k-1} \cup f$
 ;
 Update winning score: $s_k \leftarrow \text{score}(W_k)$;
end

Backward selection:

while $k > 2$ **do**
 Find the best feature to drop:
 $f \leftarrow \arg \max_f \text{score}(W_k \setminus f), \forall f \in W_k$;
 $(W_k \setminus f) \notin \mathcal{B}$;
 Update bookkeeping: $\mathcal{B} \leftarrow \mathcal{B} \cup \{W_k \setminus f\}$;
 if $\text{score}(W_k \setminus f) > s_k$ **then**
 Update winning selection:
 $W_{k-1} \leftarrow W_k \setminus f$;
 Update winning score:
 $s_{k-1} \leftarrow \text{score}(W_{k-1})$;
 $k \leftarrow k - 1$;
 else
 break ;
 end
end

$k \leftarrow k + 1$;

end

experiment, we obtained the performance of feature selections using 1 to 50 features incrementally, and selected the best feature set corresponding to the best cross-validation accuracy.

C. Model training and evaluation

Tentative feature selections were used to give , we performed nested cross-validation using SVM classifiers to obtain the accuracy scores.

In each of the outer 10-fold cross-validation loop, the data points of 90% of the individuals were used for training, on which another 10-fold cross-validation followed for parameter

tuning and cross-validation score generation. We then use the rest 10% data to obtain the test scores.

This process was done on both the original dataset from which the features were selected, and an external dataset using the selected features.

D. Feature selection evaluation

To examine the efficiency of our proposed mSFFS feature selection algorithm, we also trained and obtained the test scores through the same process, using features selected by the classical SFFS (from the `mlxtend` package [38]) (denoted by SFFS), and the top- n features ranked by SHAP using the same amount of features (denoted by SHAP).

For a wider comparison, we also evaluated various swarm-based feature selection schemes, including the binary particle swarm optimization (PSO) [39], binary Harris Hawks optimizer (BHH) [40], binary grey wolf optimization (BGW) [41], and the improved dragonfly algorithm (IDA) [42]. We used the open-sourced Zoofs library¹ with default setting to perform these swarm-based feature selections. The classification performance of feature selections obtained from these algorithms was compared with that obtained by mSFFS.

Obviously, there will be partial overlaps between various feature selections as the relevant algorithms all target some good features. To evaluate the similarity between selected feature sets, we used the Jaccard index. Given two feature selections F_1 and F_2 , the Jaccard index is given by

$$J = \frac{|F_1 \cap F_2|}{|F_1 \cup F_2|}. \quad (2)$$

We expect the Jaccard indices will be moderate between selected feature sets given by different feature selection algorithms.

To further assess the quality of selected feature schemes, we took both a qualitative approach (through visualization) and a quantitative approach (by measuring class separabilities).

1) *Visualization*: To visualize the feature selections and visually assess their potential for being used for classification, the t-distributed stochastic neighbor embedding (t-SNE) algorithm [43] is used. Specifically, given a data set X , the similarity between data points \mathbf{x}_i and \mathbf{x}_j is translated to a conditional probability density defined by

$$p_{j|i} = \frac{\exp(-\frac{\|\mathbf{x}_i - \mathbf{x}_j\|^2}{2\sigma_i^2})}{\sum_{k \neq i} \exp(-\frac{\|\mathbf{x}_i - \mathbf{x}_k\|^2}{2\sigma_i^2})}, \quad (3)$$

where σ_k is the Gaussian radius that can be automatically decided from a given perplexity value [43]. A joint probability density can be defined by including an opposite conditional as well:

$$p_{ij} = \frac{p_{i|j} + p_{j|i}}{2}. \quad (4)$$

Now suppose the data points are projected onto a low dimensionality d (usually 2 or 3 for visualization), the similarity

¹Available at <https://jaswinder9051998.github.io/zoofs/>

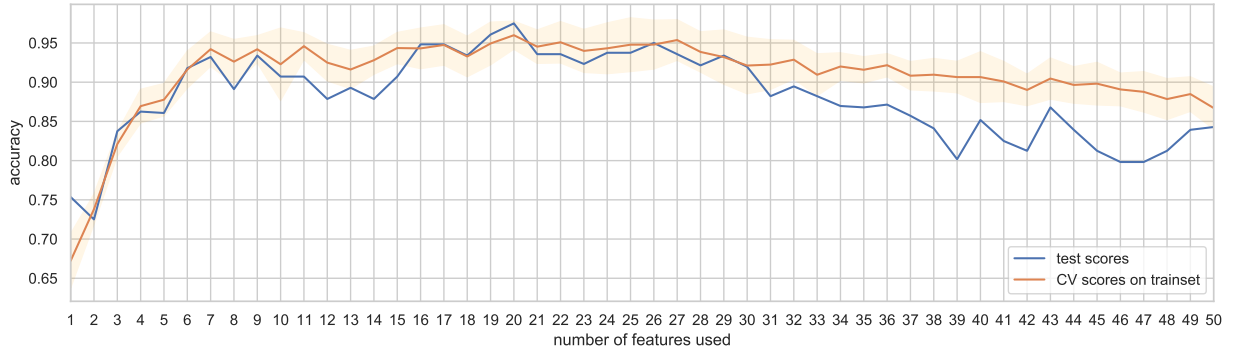


Fig. 1: Classification accuracy scores when using an increasing number of mSFFS selected features. The shadow area gives the confidence intervals of the cross-validation scores.

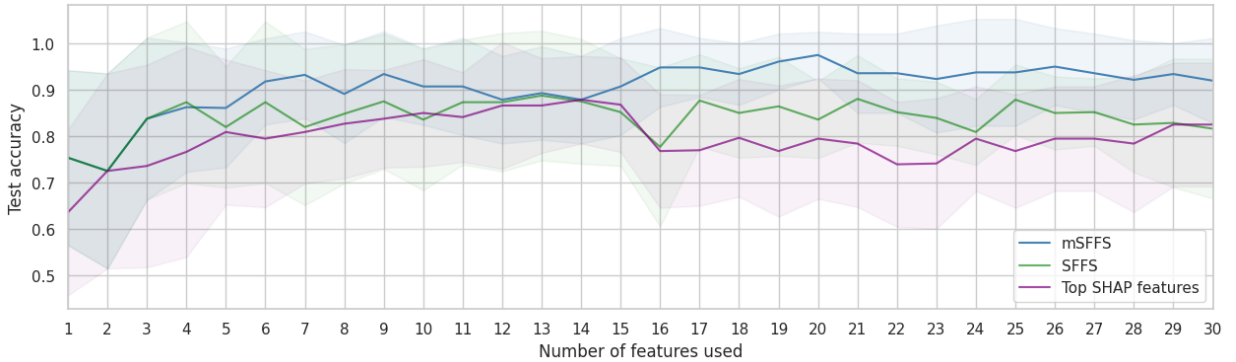


Fig. 2: Testing scores using an increasing number of features. The shadow areas represent the confidence intervals for 10-fold tests.

between points i and j can be similarly represented by the following probability density using the Student-t distribution:

$$q_{ij} = \frac{(1 + \|\mathbf{y}_i - \mathbf{y}_j\|^2)^{-1}}{\sum_k \sum_{l \neq k} (1 + \|\mathbf{y}_k - \mathbf{y}_l\|^2)^{-1}}. \quad (5)$$

To generate a good projection, the similarity relationship between data points should be maintained, hence the two joint distributions should be as close as possible. This optimization problem can be solved by employing gradient descent to minimize the Kullback-Leibler divergence (KLD) between the two joint distributions. The Scikit-learn [44] implementation of t-SNE is used in this study. The perplexity is set to 25.

2) *Measure of separability*: We use the Bhattacharyya distance as an additional metric to measure the separability of the feature selection schemes, independent from classifier choices.

Assume two normal distributions $p = N(\boldsymbol{\mu}_1, \boldsymbol{\Sigma}_1)$ and $q = N(\boldsymbol{\mu}_2, \boldsymbol{\Sigma}_2)$. The Bhattacharyya distance between them is given by

$$D_B(p, q) = \frac{1}{8}(\boldsymbol{\mu}_1 - \boldsymbol{\mu}_2)^T \boldsymbol{\Sigma}^{-1}(\boldsymbol{\mu}_1 - \boldsymbol{\mu}_2) + \frac{1}{2} \ln \left(\frac{|\boldsymbol{\Sigma}|}{\sqrt{|\boldsymbol{\Sigma}_1| |\boldsymbol{\Sigma}_2|}} \right), \quad (6)$$

where $\boldsymbol{\Sigma} = (\boldsymbol{\Sigma}_1 + \boldsymbol{\Sigma}_2)/2$. From this definition, we can see that the Bhattacharyya distance extends the Mahalanobis distance by adding an extra term that informs on the dissimilarity between the two covariance matrices. The Bhattacharyya

distance has been effectively used for optimizing feature extraction [45] and transfer learning [46].

V. RESULTS

A. Selected features

We produced feature selections of increasing dimensionality (from 1 to 50) and obtained their corresponding cross-validation scores and test accuracies (Fig. 1). According to the cross-validation curve, using 20 features produces the best mean validation score of 0.960 with a relatively small standard deviation of 0.018. This happens to be where the mean testing score peaks (0.975). We, therefore, use these 20 features as the final selected connectivity features. They are: P4-O1 theta, Fp1-F7 theta, T4-Pz theta, F4-P4 beta, F8-Cz delta, Fp1-F4 beta, T5-O1 theta, T3-T6 delta, T5-P3 delta, F8-T3 gamma, Fz-P4 gamma, F8-T4 beta, F3-F4 alpha, T3-C3 gamma, C3-T4 beta, F4-F8 alpha, Fz-F4 alpha, F8-T5 delta, Fz-Cz delta, and Fp2-F7 theta.

a) *Evolution of feature selections*: To gain some insight on the floating selection processes in both SFFS and mSFFS and how the selection outcomes evolve, the selected feature sets are displayed in Table I when the number of features increases from 1 to 20. Starting from the same first two chosen features, the feature selections of both schemes start to diverge from $k = 4$, yet maintaining some similarity to each other.

k	mSFFS		SFFS	
	Selected features	t-score	Selected features	t-score
1	P4-O1(θ)	0.754	P4-O1(θ)	0.754
2	P4-O1(θ), Fp1-F7(θ)	0.725	Fp1-F7(θ), P4-O1(θ)	0.725
3	P4-O1(θ), Fp1-F7(θ), T4-Pz(θ)	0.838	Fp1-F7(θ), P4-O1(θ), T4-Pz(θ)	0.838
4	P4-O1(θ), Fp1-F7(θ), T4-Pz(θ), F4-P4(β)	0.862	Fp1-F7(θ), P4-O1(θ), T4-Pz(θ), C3-T4(β)	0.873
5	P4-O1(θ), Fp1-F7(θ), T4-Pz(θ), F4-P4(β), C3-T4(β)	0.861	Fp1-F7(θ), P4-O1(θ), T4-Pz(θ), Fp1-F4(β), C3-T4(β)	0.820
6	P4-O1(θ), Fp1-F7(θ), T4-Pz(θ), F4-P4(β), Fp2-T4(θ), Fz-C4(δ)	0.918	Fp1-F7(θ), P4-O1(θ), T4-Pz(θ), Fp1-F4(β), Cz-T6(β), C3-T4(β)	0.873
7	P4-O1(θ), Fp1-F7(θ), T4-Pz(θ), F4-P4(β), Fp2-T4(θ), Fz-C4(δ), F8-Cz(δ)	0.932	Fp1-F7(θ), P4-O1(θ), T4-Pz(θ), Fp1-F4(β), F4-C4(δ), Cz-T6(β), C3-T4(β)	0.82
8	P4-O1(θ), Fp1-F7(θ), T4-Pz(θ), F4-P4(β), Fp2-T4(θ), Fz-C4(δ), F8-Cz(δ), T4-Pz(γ)	0.891	Fp1-F7(θ), P4-O1(θ), T4-Pz(θ), F8-T3(γ), Fp1-F4(β), F4-C4(δ), Cz-T6(β), C3-T4(β)	0.848
9	P4-O1(θ), Fp1-F7(θ), T4-Pz(θ), F4-P4(β), Fp2-T4(θ), Fz-C4(δ), F8-Cz(δ), T4-Pz(γ), Fp1-F8(δ)	0.934	Fp1-F7(θ), P4-O1(θ), T4-Pz(θ), F8-T3(γ), Fp1-F4(β), F7-P4(γ), F4-C4(δ), Cz-T6(β), C3-T4(β)	0.875
10	P4-O1(θ), Fp1-F7(θ), T4-Pz(θ), F4-P4(β), Fp2-T4(θ), Fz-C4(δ), F8-Cz(δ), T4-Pz(γ), Fp1-F8(δ), T3-P3(γ)	0.907	Fp1-F7(θ), P4-O1(θ), T4-Pz(θ), F8-T3(γ), Fp1-F4(β), F7-P4(γ), F4-C4(δ), Cz-T6(β), F8-T4(β), C3-T4(β)	0.836
11	P4-O1(θ), Fp1-F7(θ), T4-Pz(θ), F4-P4(β), Fp2-T4(θ), Fz-C4(δ), F8-Cz(δ), T4-Pz(γ), Fp1-F8(δ), T3-P3(γ), Fp1-F4(β)	0.907	Fp1-F7(θ), P4-O1(θ), T4-Pz(θ), F8-T3(γ), Fp1-F4(β), F7-P4(γ), F4-C4(δ), Cz-T6(β), F8-T4(β), C3-T4(β), C3-P3(α)	0.873
12	P4-O1(θ), Fp1-F7(θ), T4-Pz(θ), F4-P4(β), Fp2-T4(θ), Fz-C4(δ), F8-Cz(δ), T4-Pz(γ), Fp1-F8(δ), T3-P3(γ), Fp1-F4(β), C3-O1(δ)	0.879	Fp1-F7(θ), P4-O1(θ), T4-Pz(γ), T4-Pz(θ), F8-T3(γ), Fp1-F4(β), F7-P4(γ), F4-C4(δ), Cz-T6(β), F8-T4(β), C3-T4(β), C3-P3(α)	0.873
13	P4-O1(θ), Fp1-F7(θ), T4-Pz(θ), F4-P4(β), Fp2-T4(θ), Fz-C4(δ), F8-Cz(δ), T4-Pz(γ), Fp1-F8(δ), T3-P3(γ), Fp1-F4(β), C3-O1(δ), Fp1-F7(α)	0.893	Fp1-F7(θ), P4-O1(θ), T4-Pz(γ), T4-Pz(θ), F4-C3(α), F8-T3(γ), Fp1-F4(β), F7-P4(γ), F4-C4(δ), Cz-T6(β), F8-T4(β), C3-T4(β), C3-P3(α)	0.888
14	P4-O1(θ), Fp1-F7(θ), T4-Pz(θ), F4-P4(β), Fp2-T4(θ), Fz-C4(δ), F8-Cz(δ), T4-Pz(γ), Fp1-F8(δ), T3-P3(γ), Fp1-F4(β), C3-O1(δ), Fp1-F7(α), F7-P4(γ)	0.879	Fp1-F7(θ), P4-O1(θ), T4-Pz(γ), T4-Pz(θ), F4-C4(θ), F4-C3(α), F8-T3(γ), Fp1-F4(β), F7-P4(γ), F4-C4(δ), Cz-T6(β), F8-T4(β), C3-T4(β), C3-P3(α)	0.875
15	P4-O1(θ), Fp1-F7(θ), T4-Pz(θ), F4-P4(β), Fp2-T4(θ), Fz-C4(δ), F8-Cz(δ), T4-Pz(γ), Fp1-F8(δ), T3-P3(γ), Fp1-F4(β), C3-O1(δ), Fp1-F7(α), F7-P4(γ), T5-O1(θ)	0.907	Fp1-F7(θ), P4-O1(θ), T4-Pz(γ), T4-Pz(θ), F4-C4(θ), Fz-P4(γ), F4-C3(α), F8-T3(γ), Fp1-F4(β), F7-P4(γ), F4-C4(δ), Cz-T6(β), F8-T4(β), C3-T4(β), C3-P3(α)	0.852
16	P4-O1(θ), Fp1-F7(θ), T4-Pz(θ), F4-P4(β), F8-Cz(δ), Fp1-F4(β), T5-O1(θ), Fz-P4(γ), F8-T4(β), F3-F4(α), C3-T4(β), F4-F8(α), Fz-F4(α), F8-T5(δ), Fz-Cz(δ), Fp2-F7(θ)	0.948	Fp1-F7(θ), P4-O1(θ), T4-Pz(γ), T4-Pz(θ), F4-C4(θ), Fz-P4(γ), F4-C3(α), F8-T3(γ), Fp1-F4(β), F7-P4(γ), F4-C4(δ), Cz-T6(β), F4-P4(β), F8-T4(β), C3-T4(β), C3-P3(α)	0.777
17	P4-O1(θ), Fp1-F7(θ), T4-Pz(θ), F4-P4(β), F8-Cz(δ), Fp1-F4(β), T5-O1(θ), F8-T3(γ), Fz-P4(γ), F8-T4(β), F3-F4(α), C3-T4(β), F4-F8(α), Fz-F4(α), F8-T5(δ), Fz-Cz(δ), Fp2-F7(θ)	0.948	Fp1-F7(θ), P4-O1(θ), T4-Pz(γ), T4-Pz(θ), F4-C4(θ), Fp2-T4(θ), Fz-P4(γ), F4-C3(α), F8-T3(γ), Fp1-F4(β), F7-P4(γ), F4-C4(δ), Cz-T6(β), F4-P4(β), F8-T4(β), C3-T4(β), F8-Cz(δ)	0.877
18	P4-O1(θ), Fp1-F7(θ), T4-Pz(θ), F4-P4(β), F8-Cz(δ), Fp1-F4(β), T5-O1(θ), F8-T3(γ), Fz-P4(γ), F8-T4(β), F3-F4(α), T3-C3(γ), C3-T4(β), F4-F8(α), Fz-F4(α), F8-T5(δ), Fz-Cz(δ), Fp2-F7(θ)	0.934	Fp1-F7(θ), P4-O1(θ), T4-Pz(γ), T4-Pz(θ), F4-C4(θ), Fp2-T4(θ), Fz-P4(γ), F4-C3(α), F8-T3(γ), T3-C3(γ), Fp1-F4(β), F7-P4(γ), F4-C4(δ), Cz-T6(β), F4-P4(β), F8-T4(β), C3-T4(β), F8-Cz(δ)	0.850
19	P4-O1(θ), Fp1-F7(θ), T4-Pz(θ), F4-P4(β), F8-Cz(δ), Fp1-F4(β), T5-O1(θ), T5-P3(δ), F8-T3(γ), Fz-P4(γ), F8-T4(β), F3-F4(α), T3-C3(γ), C3-T4(β), F4-F8(α), Fz-F4(α), F8-T5(δ), Fz-Cz(δ), Fp2-F7(θ)	0.961	Fp1-F7(θ), P4-O1(θ), T4-Pz(γ), T4-Pz(θ), F4-C4(θ), Fp2-T4(θ), Fz-P4(γ), F4-C3(α), F8-T3(γ), T3-C3(γ), Fz-F8(δ), Fp1-F4(β), F7-P4(γ), F4-C4(δ), Cz-T6(β), F4-P4(β), F8-T4(β), C3-T4(β), F8-Cz(δ)	0.864
20	P4-O1(θ), Fp1-F7(θ), T4-Pz(θ), F4-P4(β), F8-Cz(δ), Fp1-F4(β), T5-O1(θ), T3-T6(δ), T5-P3(δ), F8-T3(γ), Fz-P4(γ), F8-T4(β), F3-F4(α), T3-C3(γ), C3-T4(β), F4-F8(α), Fz-F4(α), F8-T5(δ), Fz-Cz(δ), Fp2-F7(θ)	0.975	Fp1-F7(θ), P4-O1(θ), T4-Pz(γ), T4-Pz(θ), F4-C4(θ), Fp2-T4(θ), Fz-P4(γ), F4-C3(α), F8-T3(γ), T3-C3(γ), Fz-F8(δ), Fp1-F4(β), F7-P4(γ), F4-C4(δ), C3-O1(δ), Cz-T6(β), F4-P4(β), F8-T4(β), C3-T4(β), F8-Cz(δ)	0.836

TABLE I: Evolution of feature selection for mSFFS and SFFS when the number of features k increases from 1 to 20.

b) Jaccard indeces: Upon reaching $k = 20$, the mSFFS selection gives a Jaccard index of 0.379 to that of SFFS. It actually overlaps less with the top-20 (with the highest SHAP values) feature set, with a Jaccard index of 0.333, while the same index between SFFS and top-20 selections is 0.538. Hence mSFFS's search route further deviates from the top-20 set, allowing alternative features to be explored for inclusion that have less redundancy to existing features but larger contributions to classification.

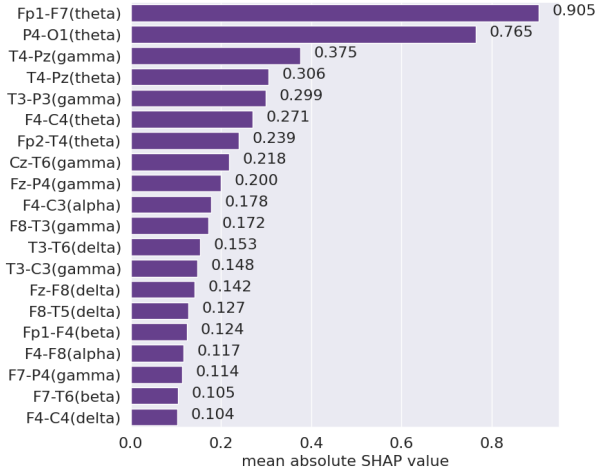
c) SHAP value comparison: The sorted, mean absolute SHAP values of the features selected by three feature selection schemes are shown in Fig. 3. The difference in the search outcome in mSFFS is also reflected here. Clearly, mSFFS does not simply favor features with large SHAP values, which may help it overcome the simple greedy nature of SFFS, allowing

small features with lesser SHAP values to be chosen and eventually contribute to better performance.

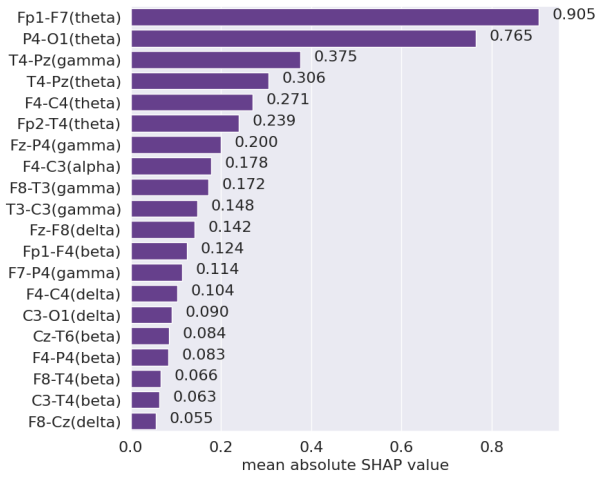
B. Classification performance

We followed the nested cross-validation process described in Section IV-C. The average cross-validation score on the training set is 0.960 (± 0.018), and the average test score is 0.975 (± 0.050) on the original knee pain dataset.

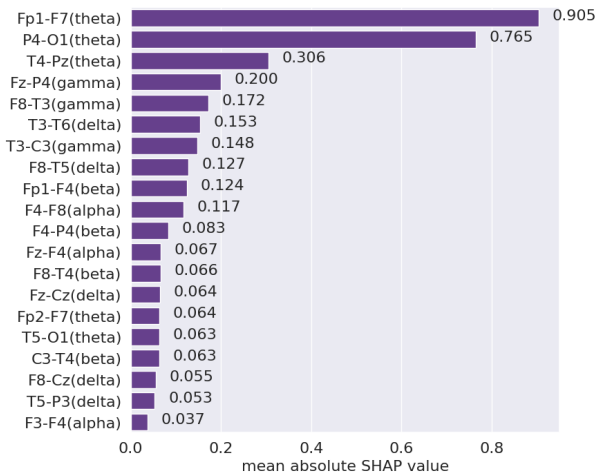
The average training score on the external chronic pain set using the selected features is 0.862 (± 0.036), and the average test score is 0.814 (± 0.123). There is a test performance drop compared to the original dataset. This could be due to the different types of chronic pain from the two datasets. The features were selected from chronic knee pain data, hence might have resulted in overfitting, whereas the external test



(a) SHAP



(b) SFFS



(c) mSFFS

Fig. 3: Mean absolute SHAP values of the features selected by three feature selection schemes: (a) top-20 SHAP; (b) SFFS, 20 features; (c) SFFS, 20 features.

set consists of neuropathic pain and other unknown types of chronic pain.

We compared the classification performance of the mSFFS

Algorithm	Feature dimensions	Accuracy
BPSO [39]	417	0.607
BHH [40]	556	0.539
BGW [41]	615	0.552
IDA [42]	404	0.602
SHAP	20	0.795
SFFS	20	0.836
mSFFS	20	0.975

TABLE II: Feature selection schemes and their testing performance in comparison.

k	mSFFS vs SFFS		mSFFS vs SHAP	
	t-statistics	p -value	t-statistics	p -value
1	0.00	1.00	1.36	0.19
2	0.00	1.00	0.00	1.00
3	0.00	1.00	1.09	0.29
4	-0.14	0.89	1.09	0.29
5	0.67	0.51	0.77	0.45
6	0.68	0.51	2.12	<i>0.05*</i>
7	1.75	0.10	2.55	<i>0.02*</i>
8	0.70	0.49	1.22	0.24
9	1.03	0.32	2.07	<i>0.05*</i>
10	1.24	0.23	1.20	0.24
11	1.60	0.56	1.39	0.18
12	0.09	0.93	0.23	0.82
13	0.09	0.93	0.56	0.58
14	0.07	0.95	0.00	1.00
15	1.06	0.30	0.81	0.43
16	2.69	<i>0.02*</i>	3.64	<i>0.00*</i>
17	1.81	0.09	3.95	<i>0.00*</i>
18	2.15	<i>0.05*</i>	2.88	<i>0.01*</i>
19	2.63	<i>0.03*</i>	3.77	<i>0.00*</i>
20	4.32	<i>0.00*</i>	3.90	<i>0.00*</i>
21	1.31	0.21	2.83	<i>0.01*</i>
22	2.24	<i>0.04*</i>	3.70	<i>0.00*</i>
23	1.81	0.09	3.00	<i>0.01*</i>
24	2.85	<i>0.01*</i>	2.66	<i>0.02*</i>
25	1.28	0.22	3.03	<i>0.01*</i>
26	2.62	<i>0.02*</i>	3.33	<i>0.00*</i>
27	2.24	<i>0.04*</i>	2.99	<i>0.01*</i>
28	2.16	<i>0.04*</i>	2.42	<i>0.03*</i>
29	2.05	<i>0.05*</i>	2.19	<i>0.04*</i>
30	1.76	0.09	1.75	0.10

TABLE III: T-test results on the testing scores obtained from mSFFS selections versus those selected by SFFS and top SHAP values over a range of dimensionality up to 30-dim. Further results are statistical insignificant, hence omitted. Dimensionalities on which mSFFS outperforms both SFFS and SHAP with statistical significance ($p \leq 0.05$) are highlighted in bold. Asterisks after p -values in italics indicate significance.

scheme with SFFS, top-20 SHAP selections, and selections given by the swarm-based schemes. None of the swarm-based feature selection schemes effectively reduced the feature dimension. SHAP and SFFS can designate a specific feature number, but their performance is worse than mSFFS. Table II gives the number of features and test accuracy from each feature selection algorithm. It can be seen that swarm-based selection methods, including BPSO, BHH, BGW and IDA, failed to find a compact feature selection, all resulting in dimensionalities larger than 400. The corresponding feature selections also performed poorly in classification, achieving accuracies hardly above 0.600.

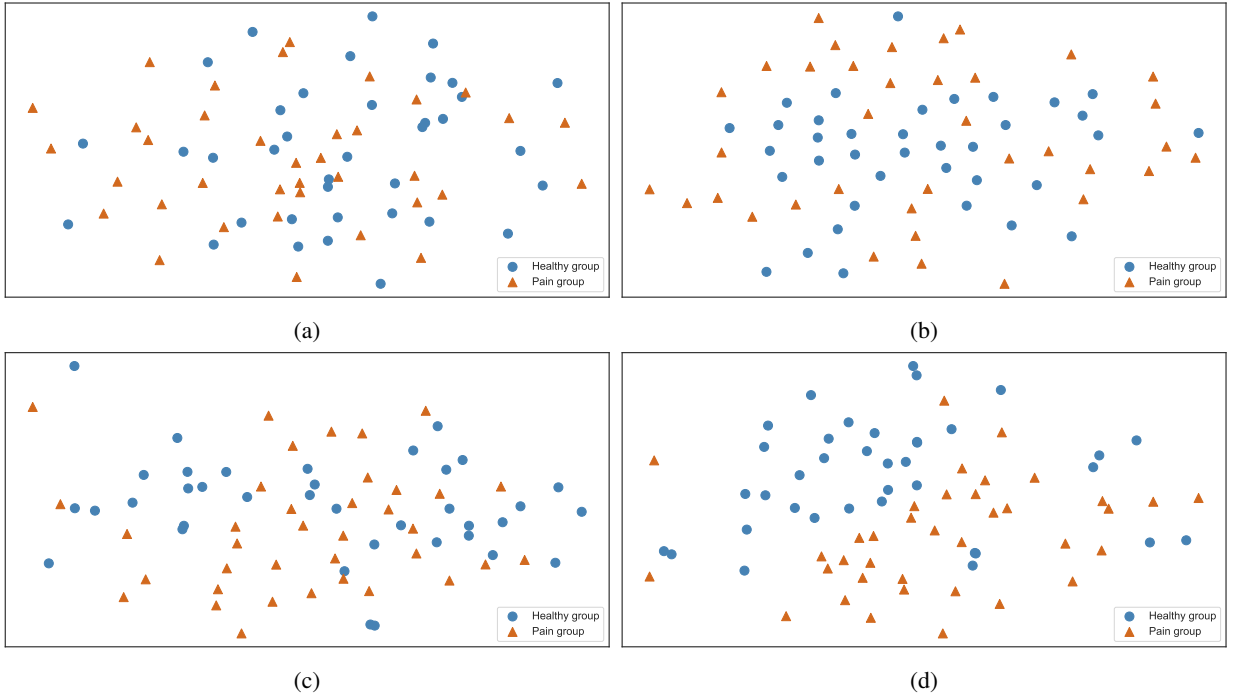


Fig. 4: Outcome of t-SNE visualization of data distributions using: (a) all 855 features; (b) 20 top-ranked SHAP features; (c) 20 features selected by SFFS; (d) 20 features selected by mSFFS.

C. Detailed evaluations

Therefore, we excluded the swarm-based feature selection schemes and only considered approaches that can effectively reduce the dimension for further analyses. Specifically, we carried out t-test on performance data, t-SNE visualization, and class separability evaluations on the SHAP selector, SFFS, and mSFFS.

a) t-test: We conducted two-sided t -tests to compare the test scores obtained from each scheme using 20 features. The results of the t -tests revealed that the comparison between mSFFS and SFFS had a t -statistics value of 4.316 and a p -value of 0.0004, indicating a statistically significant difference between the two schemes. Similarly, the comparison between mSFFS and SHAP selection yielded a statistics value of 3.896 with a p -value of 0.001, suggesting that there was also a significant difference between these two schemes. The t -test results over the range of selection dimensionality ($k = 1 \sim 30$) are detailed in Table III. On 10 out of 30 occasions the performance gains of mSFFS are statistically significant against both SFFS and SHAP.

b) t-SNE visualization: The testing performance was aligned with the t-SNE visualization outcome. Figure 4 reveals the distribution of the two-class data samples before and after feature selection. Out of the three feature schemes (mSFFS, SFFS, and SHAP), the mSFFS selected features show the clearest separation between pain and healthy participants, which demonstrates the superiority of mSFFS in selecting features that contributes to differentiating the classes.

c) Bhattacharyya separabilities: In addition to the visual assessment, we also measured the dissimilarity of the healthy and pain classes' probability distributions using the Bhat-

tacharyya distance (D_B). This is accomplished using features selected through different schemes and embedded into a 2-dimensional space by t-SNE, followed by distance calculation. The result indicates that the data characterized by mSFFS features exhibit considerably greater segregation ($D_B = 1.492$) between pain and healthy individuals when compared with SFFS ($D_B = 1.256$) and SHAP-rank ($D_B = 0.223$).

To sum up, the results and findings given above suggest that mSFFS is a more effective feature selection scheme than SFFS, SHAP-based selection, and state-of-the-art swarm-based algorithms. In general, our proposed mSFFS scheme provides feature selections with better visualization and better separability, and can achieve higher accuracies with only a few features.

VI. CONCLUSION

Despite being an important healthcare issue, chronic pain has received little data-centred treatment in the research literature. In this paper, we have demonstrated that a simple, cheap and clinically useful method of chronic pain prediction can perform on raw EEG data. This permits the development of a clinically applicable device that can detect and diagnose the presence of pain in an objective purely data-driven way with a test accuracy of 97.5% on the same dataset and 81.4% on an external dataset that contains different types of chronic pain. This is highly relevant both from a research and clinical point of view. We consider the effectiveness and compactness of the selected functional connectivity a significant advantage, as this may potentially lead to cheap hardware implementations that can carry out automatic diagnosis or neuromodulation of chronic pain.

We utilized EEG data acquired from two sources in this study. On the other hand, the so-called “domain gaps” were reported in the literature, namely, trained predictive models may have reduced generalization ability on EEGs acquired from diverse sources [47]. Another limitation of the current study is that we did not pursue a deep-learning solution owing to the small amount of data we had.

For future work, we will seek to augment our datasets by including recordings from more subjects at different sources. With data of larger amounts and more diversity available, the next step is to investigate applying deep domain adaption techniques [48], [49] and developing classification models that perform steadily across pain types and acquisition sources.

REFERENCES

- [1] J. J. Bonica, “The need of a taxonomy,” *Pain*, vol. 6, no. 3, pp. 247–248, 1979.
- [2] R.-D. Treede, W. Rief, A. Barke, Q. Aziz, M. I. Bennett, R. Benoliel, M. Cohen, S. Evers, N. B. Finnerup, M. B. First, M. A. Giamberardino, S. Kaasa, B. Korwisi, E. Kosek, P. Lavand’homme, M. Nicholas, S. Perrot, J. Scholz, S. Schug, B. H. Smith, P. Svensson, J. W. S. Vlaeyen, and S.-J. Wang, “Chronic pain as a symptom or a disease: the IASP classification of chronic pain for the international classification of diseases (ICD-11),” *Pain*, vol. 160, no. 1, pp. 19–27, Jan. 2019.
- [3] J. Scholz, N. B. Finnerup, N. Attal, Q. Aziz, R. Baron, M. I. Bennett, R. Benoliel, M. Cohen, G. Cruccu, K. D. Davis, S. Evers, M. First, M. A. Giamberardino, P. Hansson, S. Kaasa, B. Korwisi, E. Kosek, P. Lavand’homme, M. Nicholas, T. Nurmikko, S. Perrot, S. N. Raja, A. S. C. Rice, M. C. Rowbotham, S. Schug, D. M. Simpson, B. H. Smith, P. Svensson, J. W. S. Vlaeyen, S.-J. Wang, A. Barke, W. Rief, R.-D. Treede, and Classification Committee of the Neuropathic Pain Special Interest Group (NeuPSIG), “The IASP classification of chronic pain for ICD-11: chronic neuropathic pain,” *Pain*, vol. 160, no. 1, pp. 53–59, Jan. 2019.
- [4] R. Kuner and H. Flor, “Structural plasticity and reorganisation in chronic pain,” *Nat. Rev. Neurosci.*, vol. 18, no. 1, pp. 20–30, Dec. 2016.
- [5] S. E. E. Mills, K. P. Nicolson, and B. H. Smith, “Chronic pain: a review of its epidemiology and associated factors in population-based studies,” *Br. J. Anaesth.*, vol. 123, no. 2, pp. e273–e283, Aug. 2019.
- [6] O. Moriarty, B. E. McGuire, and D. P. Finn, “The effect of pain on cognitive function: a review of clinical and preclinical research,” *Prog. Neurobiol.*, vol. 93, no. 3, pp. 385–404, Mar. 2011.
- [7] H. Breivik, B. Collett, V. Ventafridda, R. Cohen, and D. Gallacher, “Survey of chronic pain in Europe: prevalence, impact on daily life, and treatment,” *Eur. J. Pain*, vol. 10, no. 4, pp. 287–333, May 2006.
- [8] Y. Zheng, T. Zhang, X. Yang, Z. Feng, F. Qiu, G. Xin, J. Liu, F. Nie, X. Jin, and Y. Liu, “A survey of chronic pain in China,” *Libyan J. Med.*, vol. 15, no. 1, p. 1730550, Dec. 2020.
- [9] E. N. Mutubuki, Y. Beljon, E. T. Maas, F. J. P. M. Huygen, R. W. J. G. Ostelo, M. W. van Tulder, and J. M. van Dongen, “The longitudinal relationships between pain severity and disability versus health-related quality of life and costs among chronic low back pain patients,” *Quality of Life Research*, vol. 29, no. 1, pp. 275–287, Jan. 2020.
- [10] GBD 2017 Disease and Injury Incidence and Prevalence Collaborators, “Global, regional, and national incidence, prevalence, and years lived with disability for 354 diseases and injuries for 195 countries and territories, 1990–2017: a systematic analysis for the global burden of disease study 2017,” *Lancet*, vol. 392, no. 10159, pp. 1789–1858, Nov. 2018.
- [11] D. J. Gaskin and P. Richard, “The economic costs of pain in the United States,” *Journal of Pain*, vol. 13, no. 8, pp. 715–724, Aug. 2012.
- [12] M. W. van Tulder, B. W. Koes, and L. M. Bouter, “A cost-of-illness study of back pain in the netherlands,” *Pain*, vol. 62, no. 2, pp. 233–240, Aug. 1995.
- [13] J. Dahlhamer, J. Lucas, C. Zelaya, R. Nahin, S. Mackey, L. DeBar, R. Kerns, M. Von Korff, L. Porter, and C. Helmick, “Prevalence of chronic pain and high-impact chronic pain among adults - United States, 2016,” *MMWR Morb. Mortal. Wkly. Rep.*, vol. 67, no. 36, pp. 1001–1006, Sep. 2018.
- [14] T. Jackson, S. Thomas, V. Stabile, X. Han, M. Shotwell, and K. McQueen, “Prevalence of chronic pain in low-income and middle-income countries: a systematic review and meta-analysis,” *Lancet*, vol. 385 Suppl 2, p. S10, Apr. 2015.
- [15] T. D. Wager, L. Y. Atlas, M. A. Lindquist, M. Roy, C.-W. Woo, and E. Kross, “An fMRI-based neurologic signature of physical pain,” *N. Engl. J. Med.*, vol. 368, no. 15, pp. 1388–1397, Apr. 2013.
- [16] C. L. Stucky, M. S. Gold, and X. Zhang, “Mechanisms of pain,” *Proc. Natl. Acad. Sci. U. S. A.*, vol. 98, no. 21, pp. 11 845–11 846, Oct. 2001.
- [17] M. P. Jensen, M. A. Day, and J. Miró, “Neuromodulatory treatments for chronic pain: efficacy and mechanisms,” *Nat. Rev. Neurol.*, vol. 10, no. 3, pp. 167–178, Mar. 2014.
- [18] J. A. Kim, R. L. Bosma, K. S. Hemington, A. Rogachov, N. R. Osborne, J. C. Cheng, B. T. Dunkley, and K. D. Davis, “Sex-differences in network level brain dynamics associated with pain sensitivity and pain interference,” *Human Brain Mapping*, vol. 42, no. 3, pp. 598–614, 2021.
- [19] J. A. Kim, R. L. Bosma, K. S. Hemington, A. Rogachov, N. R. Osborne, J. C. Cheng, J. Oh, B. T. Dunkley, and K. D. Davis, “Cross-network coupling of neural oscillations in the dynamic pain connectome reflects chronic neuropathic pain in multiple sclerosis,” *NeuroImage: Clinical*, vol. 26, p. 102230, 2020.
- [20] J. A. Kim and K. D. Davis, “Neural oscillations: understanding a neural code of pain,” *The Neuroscientist*, vol. 27, no. 5, pp. 544–570, 2021.
- [21] D. De Ridder, S. Perera, and S. Vanneste, “State of the art: Novel applications for cortical stimulation,” *Neuromodulation*, vol. 20, no. 3, pp. 206–214, Apr. 2017.
- [22] S. Vanneste, J.-J. Song, and D. De Ridder, “Thalamocortical dysrhythmia detected by machine learning,” *Nature Communications*, vol. 9, no. 1, pp. 1–13, 2018.
- [23] T. Nezam, R. Boostani, V. Abootalebi, and K. Rastegar, “A novel classification strategy to distinguish five levels of pain using the EEG signal features,” *IEEE Transactions on Affective Computing*, vol. 12, no. 1, pp. 131–140, 2018.
- [24] A. Vuckovic, V. J. F. Gallardo, M. Jarjees, M. Fraser, and M. Purcell, “Prediction of central neuropathic pain in spinal cord injury based on EEG classifier,” *Clinical Neurophysiology*, vol. 129, no. 8, pp. 1605–1617, 2018.
- [25] V. Vijayakumar, M. Case, S. Shirinpour, and B. He, “Quantifying and characterizing tonic thermal pain across subjects from EEG data using random forest models,” *IEEE Transactions on Biomedical Engineering*, vol. 64, no. 12, pp. 2988–2996, 2017.
- [26] H. van Dijk, G. van Wingen, D. Denys, S. Olbrich, R. van Ruth, and M. Arns, “The two decades brainclinics research archive for insights in neurophysiology (tdbrain) database,” *Scientific data*, vol. 9, no. 1, pp. 1–10, 2022.
- [27] M. Jas, D. A. Engemann, Y. Bekhti, F. Raimondo, and A. Gramfort, “Autoreject: Automated artifact rejection for meg and eeg data,” *NeuroImage*, vol. 159, pp. 417–429, 2017.
- [28] F. Perrin, O. Bertrand, and J. Pernier, “Scalp current density mapping: value and estimation from potential data,” *IEEE Transactions on Biomedical Engineering*, no. 4, pp. 283–288, 1987.
- [29] F. Perrin, J. Pernier, O. Bertrand, and J. F. Echallier, “Spherical splines for scalp potential and current density mapping,” *Electroencephalography and Clinical Neurophysiology*, vol. 72, no. 2, pp. 184–187, 1989.
- [30] M. X. Cohen, *Analyzing neural time series data: theory and practice*. MIT Press, 2014.
- [31] J. Kayser and C. E. Tenke, “On the benefits of using surface laplacian (current source density) methodology in electrophysiology,” *International journal of psychophysiology: official journal of the International Organization of Psychophysiology*, vol. 97, no. 3, p. 171, 2015.
- [32] R. Bruña, F. Maestú, and E. Pereda, “Phase locking value revisited: teaching new tricks to an old dog,” *Journal of neural engineering*, vol. 15, no. 5, p. 056011, 2018.
- [33] A. Gramfort, M. Luessi, E. Larson, D. A. Engemann, D. Strohmeier, C. Brodbeck, R. Goj, M. Jas, T. Brooks, L. Parkkonen, and M. S. Hämläinen, “MEG and EEG data analysis with MNE-Python,” *Frontiers in Neuroscience*, vol. 7, no. 267, pp. 1–13, 2013.
- [34] P. Pudil, J. Novovičová, and J. Kittler, “Floating search methods in feature selection,” *Pattern Recognition Letters*, vol. 15, no. 11, pp. 1119–1125, 1994.
- [35] S. M. Lundberg and S.-I. Lee, “A unified approach to interpreting model predictions,” in *Advances in Neural Information Processing Systems 30*, I. Guyon, U. V. Luxburg, S. Bengio, H. Wallach, R. Fergus, S. Vishwanathan, and R. Garnett, Eds. Curran Associates, Inc., 2017, pp. 4765–4774.
- [36] T. Chen and C. Guestrin, “XGBoost: A scalable tree boosting system,” in *Proceedings of the 22nd ACM SIGKDD International Conference on*

- Knowledge Discovery and Data Mining*, ser. KDD '16. New York, NY, USA: Association for Computing Machinery, 2016, p. 785–794.
- [37] G. James, D. Witten, T. Hastie, and R. Tibshirani, *An Introduction to Statistical Learning: with Applications in R*, 2nd ed. Springer, 2021.
- [38] S. Raschka, “MLxtend: Providing machine learning and data science utilities and extensions to python’s scientific computing stack,” *The Journal of Open Source Software*, vol. 3, no. 24, Apr. 2018.
- [39] B. Tran, B. Xue, and M. Zhang, “Overview of particle swarm optimisation for feature selection in classification,” in *Simulated Evolution and Learning: 10th International Conference, SEAL 2014, Dunedin, New Zealand, December 15-18, 2014. Proceedings 10*. Springer, 2014, pp. 605–617.
- [40] T. Thaher, A. A. Heidari, M. Mafarja, J. S. Dong, and S. Mirjalili, “Binary harris hawks optimizer for high-dimensional, low sample size feature selection,” *Evolutionary Machine Learning Techniques: Algorithms and Applications*, pp. 251–272, 2020.
- [41] E. Emary, H. M. Zawbaa, and A. E. Hassanien, “Binary grey wolf optimization approaches for feature selection,” *Neurocomputing*, vol. 172, pp. 371–381, 2016.
- [42] A. I. Hammouri, M. Mafarja, M. A. Al-Betar, M. A. Awadallah, and I. Abu-Doush, “An improved dragonfly algorithm for feature selection,” *Knowledge-Based Systems*, vol. 203, p. 106131, 2020.
- [43] L. van der Maaten and G. Hinton, “Visualizing data using t-SNE,” *Journal of Machine Learning Research*, vol. 9, no. 86, pp. 2579–2605, 2008.
- [44] F. Pedregosa, G. Varoquaux, A. Gramfort, V. Michel, B. Thirion, O. Grisel, M. Blondel, P. Prettenhofer, R. Weiss, V. Dubourg, J. Vanderplas, A. Passos, D. Cournapeau, M. Brucher, M. Perrot, and E. Duchesnay, “Scikit-learn: Machine learning in Python,” *Journal of Machine Learning Research*, vol. 12, pp. 2825–2830, 2011.
- [45] E. Choi and C. Lee, “Feature extraction based on the Bhattacharyya distance,” *Pattern Recognition*, vol. 36, no. 8, pp. 1703–1709, Aug. 2003.
- [46] M. Pándy, A. Agostinelli, J. Uijlings, V. Ferrari, and T. Mensink, “Transferability estimation using Bhattacharyya class separability,” in *2022 IEEE/CVF Conference on Computer Vision and Pattern Recognition (CVPR)*, 2022, pp. 9162–9172.
- [47] X. Chai, Q. Wang, Y. Zhao, Y. Li, D. Liu, X. Liu, and O. Bai, “A fast, efficient domain adaptation technique for cross-domain electroencephalography(EEG)-based emotion recognition,” *Sensors (Basel)*, vol. 17, no. 5, May 2017.
- [48] J. Hou, X. Ding, J. D. Deng, and S. Cranefield, “Deep adversarial transition learning using cross-grafted generative stacks,” *Neural Networks*, vol. 149, pp. 172–183, 2022.
- [49] Q. Wang, F. Meng, and T. P. Breckon, “Data augmentation with normae and selective pseudo-labelling for unsupervised domain adaptation,” *Neural Networks*, vol. 161, pp. 614–625, 2023.